

Wavelength-Resolved Optical Extinction Measurements of Aerosols Using Broad-Band Cavity-Enhanced Absorption Spectroscopy over the Spectral Range of 445–480 nm

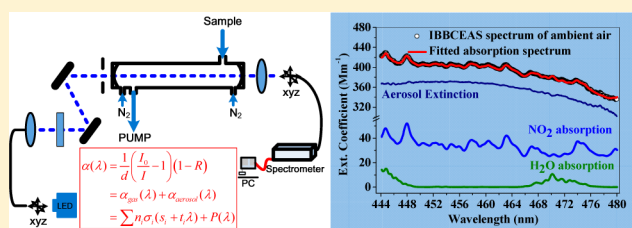
Weixiong Zhao,[†] Meili Dong,[†] Weidong Chen,[‡] Xuejun Gu,[†] Changjin Hu,[†] Xiaoming Gao,[†] Wei Huang,^{*,†} and Weijun Zhang^{*,†}

[†]Anhui Institute of Optics and Fine Mechanics, Chinese Academy of Sciences, Hefei 230031, Anhui, China

[‡]Laboratory of Physical Chemistry of the Atmosphere, Université du Littoral Côte d'Opale, 189A Avenue Maurice Schumann, 59140 Dunkerque, France

Supporting Information

ABSTRACT: Despite the significant progress in the measurements of aerosol extinction and absorption using spectroscopy approaches such as cavity ring-down spectroscopy (CRDS) and photoacoustic spectroscopy (PAS), the widely used single-wavelength instruments may suffer from the interferences of gases absorption present in the real environment. A second instrument for simultaneous measurement of absorbing gases is required to characterize the effect of light extinction resulted from gases absorption. We present in this paper the development of a blue light-emitting diode (LED)-based incoherent broad-band cavity-enhanced spectroscopy (IBBCEAS) approach for broad-band measurements of wavelength-resolved aerosol extinction over the spectral range of 445–480 nm. This method also allows for simultaneous measurement of trace gases absorption present in the air sample using the same instrument. On the basis of the measured wavelength-dependent aerosol extinction cross section, the real part of the refractive index (RI) can be directly retrieved in a case where the RI does not vary strongly with the wavelength over the relevant spectral region. Laboratory-generated monodispersed aerosols, polystyrene latex spheres (PSL) and ammonium sulfate (AS), were employed for validation of the RI determination by IBBCEAS measurements. On the basis of a Mie scattering model, the real parts of the aerosol RI were retrieved from the measured wavelength-resolved extinction cross sections for both aerosol samples, which are in good agreement with the reported values. The developed IBBCEAS instrument was deployed for simultaneous measurements of aerosol extinction coefficient and NO₂ concentration in ambient air in a suburban site during two representative days.



Atmospheric aerosol particles play important roles in climate, atmospheric environment, and human health. The aerosol optical properties are closely related to the aerosol fundamental physiochemical characteristics. The in situ characterization of aerosol optical properties is crucial for better understanding of the direct climate effect of aerosols.^{1,2}

New instruments have recently been developed for accurate measurement of aerosol key optical parameters, such as absorption, scattering, and extinction coefficients. Two optical methods, photoacoustic spectroscopy (PAS) and cavity ring-down spectroscopy (CRDS), are increasingly used for aerosol absorption and extinction measurements in aircraft or ground-based platform.^{1,3,4}

Cavity ring-down spectroscopy uses high-finesse optical cavities to realize long effective optical path lengths of up to several kilometers in a compact resonant cavity (with a base length of ~1 m), which provides an extreme sensitivity (with detection limits less than 1 Mm⁻¹, 1 Mm⁻¹ = 1 × 10⁻⁸ cm⁻¹) necessary for aerosol extinction measurements. This kind of CRDS-based instrument is now widely used for both laboratory and field measurements of aerosol optical properties.^{4–18} The

photoacoustic technique, based on the measurements of sound waves generated by photoacoustic effect with a microphone, is a direct method for aerosol absorption coefficient measurement, with a typical sensitivity of better than 1 Mm⁻¹. After more than 30 years of development, the photoacoustic spectroscopy is now a widespread and practical tool for aerosol absorption measurement.⁴ The combination of CRDS and PAS permits for the in situ determination of the aerosol signal scattering albedo without any change of the state of aerosol particles.

However, these single-wavelength CRDS or PAS instruments may suffer from the interferences of the gas-phase absorption which contributes to the measured extinction. The major gas absorption contribution in the visible spectral region is resulted from nitrogen dioxide (NO₂) absorption: it contributes an optical extinction of ~0.33 Mm⁻¹/ppbv at 532 nm, and about 1.8 Mm⁻¹/ppbv at 440 nm. Its absorption effect on aerosol extinction measurement is hence significant and must be well

Received: October 31, 2012

Accepted: January 15, 2013

Published: January 15, 2013

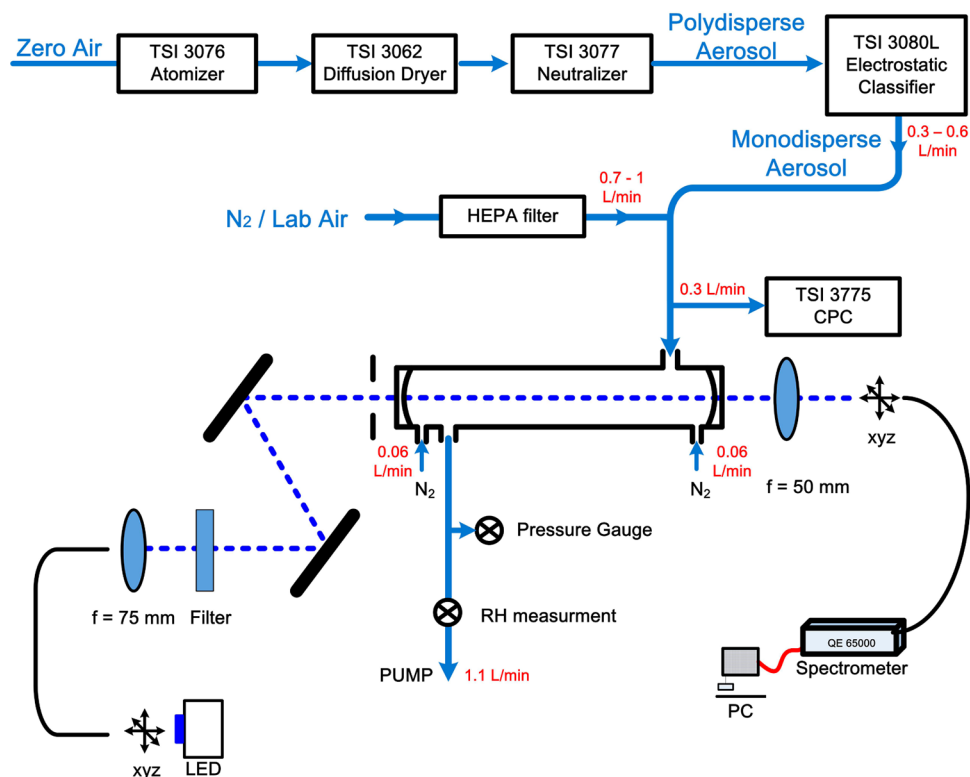


Figure 1. Schematic diagram of the developed blue LED-based IBBCEAS spectrometer and the laboratory aerosols generation system.

taken into account. The commonly used method is to perform complementary measurement of filtered air, where particles are removed from the sample by an efficient filter (the absorbing gas is presumed to be unaffected by the filter). The difference of the two measurements (with and without aerosol contribution) would allow for determination of the extinction coefficient resulted only from aerosol. However, the concentration of NO_2 is more variable depending on the distance from the source, which varies rapidly from several parts per billion by volume to several hundreds of parts per billion by volume. Under this condition, the measurement of extinction by only one CRDS instrument is not enough; usually, a second instrument or gas-phase reference channels for simultaneous NO_2 measurements are required to compensate for the influence of gas absorption induced optical extinction.¹

In this paper, we report on the development of a blue light-emitting diode (LED)-based incoherent broad-band cavity-enhanced absorption spectroscopy (IBBCEAS) approach for broad-band measurements of wavelength-dependent aerosol extinction. IBBCEAS, first proposed by Fiedler et al.,¹⁹ belongs to a class of methods using high-finesse optical cavities. The main advantage of a broad-band method over single-wavelength CRDS is its capacity of simultaneous measurement of multiple species because of the use of a broad-band light source. A spectral fitting algorithm allows one to retrieve the concentrations of multiple absorbers. We demonstrate that the IBBCEAS technique provides a robust method for simultaneous quantitative measurement of both aerosol extinction coefficients and trace gases concentration. In this manner, the gas-phase absorption can be well taken into account in aerosol extinction determination using a single analytical instrument. The developed IBBCEAS instrument was deployed for environmental air measurements of aerosol extinction coef-

ficient as well as NO_2 concentration, during two representative days (cloudy and clear day, respectively).

Compared to the single-wavelength CRDS approach, measurement of broad-band wavelength-resolved aerosol cross section using IBBCEAS provided an alternative method for retrieval of the real part of the aerosol complex refractive index (RI, $m = n + ik$, where n and k corresponds to light scattering and absorption by aerosol, respectively) from measured extinction. For many types of aerosol particles, there are no obvious extinction structures over the spectral region of several tens of nanometers and RI could be considered invariant with wavelength. In this case, for RI retrieval using single-wavelength CRDS-based instruments, a series of CRDS spectra with different given size parameters ($x = \pi D/\lambda$) needs to be measured in order to obtain a robust fit. However, in many applications, in particular for aerosol particles with small diameter, it is difficult to perform an entire set of measurements for different particle sizes because a large x is unachievable, whereas the IBBCEAS method, based on the broad-band measurements of wavelength-resolved extinction cross section, may provide a faster and more robust way for RI retrieval. In the present work involving polystyrene latex spheres (PSL) and ammonium sulfate (AS) particles, the RI does not vary strongly with wavelength over the selected wavelength region; the wavelength dispersion in the RI could be negligible. The extinction cross section is a function of only particle diameter (D) and RI (n , k). Given that k is fixed, the real part of RI, n , could be retrieved from the wavelength-resolved extinction cross section measured over a broad-band wavelength range for a single-particle diameter.

Although some papers have reported the application of IBBCEAS to aerosol extinction measurements,^{20–22} this is, to our knowledge, the first experimental attempt to quantify the refractive index of aerosols based on the wavelength-resolved

aerosol optical extinction measurements by IBBCEAS. The retrieved RI values of the laboratory-generated monodispersed PSL and AS are in good agreement with the literature reported results.

EXPERIMENTAL SECTION

IBBCEAS Spectrometer. A scheme of the IBBCEAS setup developed in the present work is shown in Figure 1. The broadband radiation was provided by a blue LED (LedEngin LZ110B200) with an emission spectrum peaked at 460 nm. The LED was mounted on a Peltier heat sink to stabilize its emission intensity. Light was coupled directly from the LED into a 600 μm core diameter and 0.22 numerical aperture multimode fiber (Ocean optics). The emerging light beam from the fiber was focused by a 75 mm focal length achromatic planoconvex lens to the center of a high-finesse optical cavity. A band-pass filter, centered at 450 nm with a full width at half-maximum (fwhm) of 40 nm (Thorlabs FB 450–40), was located in front of the cavity.

The optical cavity was made of a 102 cm long quartz tube with an inner diameter of 25 mm, closed with two highly reflective mirrors (LGR, 0.8 in. diameter, 6 m radius of curvature, $R > 99.99\%$ between 415 and 465 nm). Each mirror was isolated from the sample flow by a purge volume that was continuously flushed with high-purified nitrogen at a rate of 60 standard cubic centimeters (SCCM) to prevent degradation of the mirror reflectivity by deposition of aerosols. The distance from the inlet to the outlet was about 70 cm. The sample was continuously flowed through the cavity cell at atmospheric pressure (~ 99 kPa) at a flow rate of 1.1 L/min. Stability of the pressure in the cavity, monitored with a pressure gauge, was better than 10 Pa. NO_2 concentration was monitored with a NO_x analyzer (Thermo 42i), and the particle number concentration was monitored by a condensation particle counter (CPC, TSI 3775). Temperature and relative humidity were measured with a hygrometer humidity sensor (Rotronic, model HC2).

Light emerging from the cavity was collected with a 50 mm focal length achromatic lens and coupled into a multimode optical fiber with a 500 μm core diameter and 0.22 numerical apertures. The output of the fiber was directly connected to a spectrometer (Ocean Optics QE65000) with a slit width of 100 μm resulting in a spectral resolution of 0.4 nm over the wavelength range of 412–487 nm.

Laboratory Generation and Classification of Aerosols. Measurements of aerosol extinction coefficient by the IBBCEAS instrument was tested and validated with laboratory-generated aerosol samples. Aqueous solutions of the interested compounds were nebulized using a TSI constant output atomizer (TSI-3076) with purified compressed air from a zero air generator (Thermo 111). Polydisperse distribution of droplets was generated in the present work. The resulting droplets are dried with a silica gel column dryer (TSI 3062) and then neutralized with an aerosol neutralizer (TSI 3077) to obtain an equilibrium charge distribution. A monodisperse distribution is generated by an electrostatic classifier (TSI differential mobility analyzer, DMA 3080L). Size-selected aerosols were then diluted with dry N_2 (for the measurement of polystyrene spheres extinction) or diluted with particle-free air (to obtain a mixture of ammonium sulfate aerosol and NO_2 for performance evaluation of simultaneous retrieval of aerosol extinction and trace gases absorption). A 1.4 SLPM (standard liters per minute) flow of such samples were directed into the

IBBCEAS cell and the CPC (TSI 3775) for optical extinction measurements.

RESULTS AND DISCUSSION

Data Retrieval Processing. The IBBCEAS method is based on the measurements of light intensities transmitted through a high-finesse optical cavity. The optical extinction coefficient $\alpha(\lambda)$ due to the sample present inside the cavity can be expressed as follows:

$$\alpha(\lambda) = \alpha_{\text{aerosol}}(\lambda) + \alpha_{\text{gas}}(\lambda) = \frac{1}{d} \left(\frac{I_0(\lambda)}{I(\lambda)} - 1 \right) (1 - R(\lambda)) \quad (1)$$

where $R(\lambda)$ is the mirror effective reflectivity, d is the cavity length in which the absorber is present in the cavity, and $I_0(\lambda)$ and $I(\lambda)$ are the light intensities transmitted through the cavity without and with samples, respectively. There are two components in the measured extinction, $\alpha_{\text{aerosol}}(\lambda)$ and $\alpha_{\text{gas}}(\lambda)$, corresponding to the extinction coefficients related to aerosol and gas absorption, respectively.

According to eq 1, the aerosol extinction could be deduced from the measurements of a sample of aerosol in air (containing α_{aerosol} and α_{gas}) and the measurements of a particle-free air sample (containing only α_{gas} , where aerosols were removed by a highly efficient particle filter).²³ Utilization of a filter for sampling is an important issue that should be seriously addressed. Combined with wall loss problems, this method might introduce artifact production and chemical interference which shall affect the measurements.

In this work, the effect of trace gas absorption was quantitatively characterized by simultaneous measurement of gas absorption and aerosol extinction by using a single IBBCEAS approach. The aerosol extinction and trace gases concentrations are retrieved by using the following equation:

$$\alpha(\lambda) = \sum n_i \sigma_i(s_i + t_i \lambda) + P(\lambda) \quad (2)$$

where n_i and σ_i are the number density and the absolute absorption cross section for the i th absorber, respectively. s_i and t_i are the shift and stretch coefficients for each absorber in order to reconstruct an accurate wavelength calibration. This method is similar to that widely used in the software DOASIS²⁴ and QDOAS.²⁵ The polynomial offset $P(\lambda)$, varying from linear to fifth order, is used to account for variation in spectral background which includes wavelength-dependent attenuation by aerosol extinction and spectral baseline drift (which can be considered as system drift in the extinction measurement). For a particle-free sample, $P(\lambda)$ merely represents the spectral baseline drift including baseline variation due to Rayleigh scattering of air and unspecified background change in the spectra related to unstable LED emission or unstable dark current variation in the CCD spectrometer. For this purpose, the high performance of an IBBCEAS system is required for high-accuracy measurements of aerosol extinction such that the background drift could be negligible in comparison with the measured aerosol extinction.

For quantitative analysis, the mirror reflectivity should be experimentally determined, which can be performed by (1) measurement of cavity ring-down time or phase shift,²⁶ (2) measurement of the absorption spectrum of an absorber with known concentration and known absorption cross section,^{27–30} or (3) addition of gases with different Rayleigh cross sections.³¹ In the present work, the mirror reflectivity was calibrated using

the third method. The spectral profile of the mirror reflectivity was deduced from the difference in the transmitted intensities of N_2 and CO_2 related to Rayleigh scattering. The advantage of this method is that the Rayleigh extinction varies slowly with wavelength and provides a smooth mirror reflectivity spectrum over the whole working spectral region.^{31,32}

The cavity was flushed with N_2 and CO_2 at 1.1 L/min rate for half an hour for each species, before the measurements of its Rayleigh scattering spectra, until the transmitted light intensity attained a stable value. The Rayleigh cross sections used for the mirror reflectivity calculation were reported by Naus and Ubachs³³ and Snee and Ubachs,³⁴ with an experimental uncertainty of 1% for N_2 and 4% for CO_2 . The mirror reflectivity was found to be about 99.98% at 460 nm (Supporting Information Figure S1). During the process of mirror reflectivity calibration, the N_2 flow for purging the cavity mirror was turned off and the cavity was fully occupied with N_2 and CO_2 . During the measurements of NO_2 and aerosol, purging N_2 was continuously used which shortened the effective path length d . The effective path length was determined in such way that it was scaled to match the absorption spectrum of O_2-O_2 dimer.³⁵ A path length of 73.75 cm, by multiplying the distance between two cavity mirrors (102 cm) by a factor of 0.723, was thus determined and used for further data analyses.

Instrument Stability and Detection Limits. Measurement sensitivity of the developed IBBCEAS spectrometer was evaluated using particle-free air sample. The mirror reflectivity inferred by measuring the Rayleigh scattering spectra of N_2 and CO_2 is shown in Supporting Information Figure S1. Cavity throughput intensity is also given as reference. The mask indicates the fit spectral region. A representative of data retrieval is shown in Figure 2a. The acquisition time for each spectral data was 9 s (1.5 s integrating time, and six spectra averaging). The used NO_2 reference cross section was from the high-resolution absorption cross sections reported by Vandaele et al.,³⁶ convoluted with the slit function of the spectrometer at 294 K. The measurement sensitivity of NO_2 concentration was estimated to be $1.45 \times 10^{-9} \text{ cm}^{-1}$ (corresponding to 1σ of the spectral fit residual), which led to a detection limit of 83 pptv (parts per trillion by volume). The detection limit can be also inferred from the histograms distribution of the NO_2 concentration measurements (Supporting Information Figure S2).³⁷ The 1σ sample standard deviation of the histograms showing NO_2 distribution indicates an absolute detection limit of 96.8 pptv, which is consistent with the value estimated of 83 pptv estimated using 1σ fit residual.

A fourth-order polynomial $P(\lambda)$ was used to retrieve spectral background. The drift of 3 Mm^{-1} , which arose from Rayleigh scattering of air and potential variation in LED emission, corresponds to a fractional decrease of about 1.0% in the measurement of I to I_0 . The smooth background illustrated the good LED stability.

An Allan variance analysis was carried out to evaluate the optical system stability (and hence the maximum averaging time for the minimum detection limit) of the IBBCEAS spectrometer. A time series of 1000 absorption spectra was recorded spanning 2.5 h when the cavity was flushed with N_2 . The first N_2 measurement was used as the $I_0(\lambda)$ spectrum. Each spectrum was fitted to eq 2 to retrieve the NO_2 concentration and the background drifts $P(\lambda)$. $P(\lambda)$ at three different wavelengths (447.8, 458.55, and 468.86 nm) are shown in the upper panel of Figure 2b. As can be seen, the

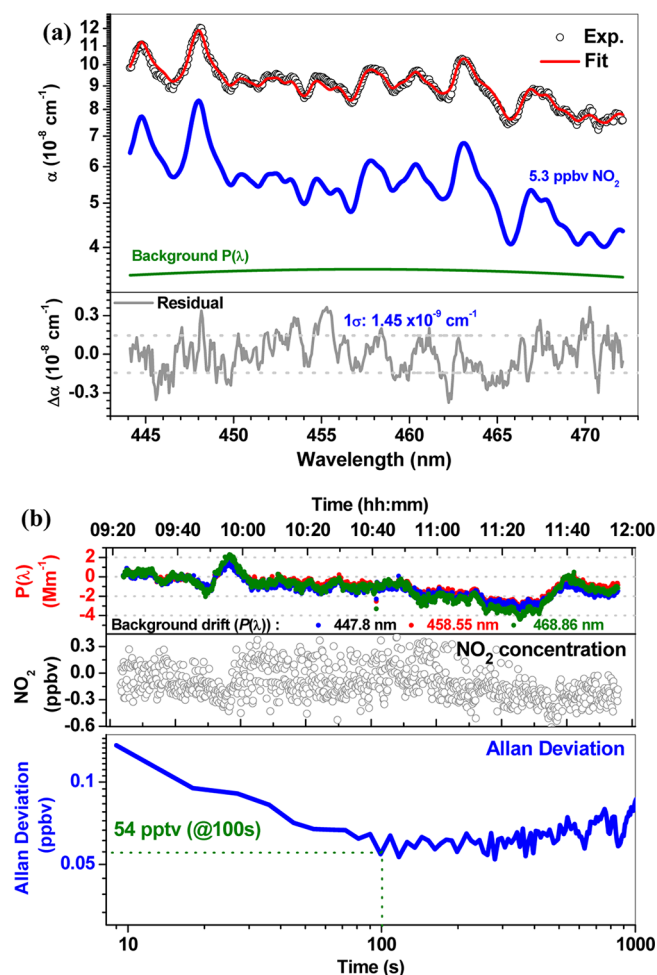


Figure 2. (a) Example of α_{abs} determination for a single measurement of an NO_2 spectrum. The experimental data and the fit are reported in the open black circles and red line, respectively. A spectral reference of 5.3 ppbv NO_2 absorption spectrum and a background $P(\lambda)$, both deduced from the fit with eq 2, are shown in blue and olive lines, respectively. The corresponding fit residual is shown in the lower panel. A 1σ detection limit of $1.45 \times 10^{-9} \text{ cm}^{-1}$ is achieved with 9 s acquire time (1.5 s integration time and six spectra averaging). (b) Time series of absorption spectra when the cavity was purged with nitrogen (1000 measurements of $I(\lambda)$, 9 s each, total acquisition time 2.5 h). The data were processed with eq 2. The first nitrogen transmitted spectral was chosen as $I_0(\lambda)$. Upper panel: background $P(\lambda)$ at three different wavelengths of 447.8, 458.55, and 468.86 nm. Middle panel: retrieved NO_2 concentration. Lower panel: Allan deviation plots for NO_2 measurements, close to a flicker noise. The minima (~ 54 pptv) in the Allan plots indicate the optimum average times (~ 100 s) for optimum detection performance.

background drifts at different wavelengths show the same trends. The long-term stability over ~ 2.5 h (1σ standard deviation of the background drift) was better than 1 Mm^{-1} , and the short-term stability (~ 20 min) was better than 0.3 Mm^{-1} .

Retrieval of NO_2 concentration and the corresponding Allan plots are shown in the middle and lower panels of Figure 2b, respectively. The minima in the Allan plots indicate the optimum averaging time for optimum detection performance. The inferred 1σ detection limit of NO_2 is 54 pptv in 100 s.

Measurements of Laboratory-Generated Particles. Performance of the IBBCEAS system for use in aerosol extinction measurement was evaluated using laboratory-

generated aerosols, PSL (Thermo) and AS, both with well-known refractive indexes.

An experimentally measured wavelength-dependent spectrum of the extinction cross section for 300 nm diameter PSL is shown in Figure 3a. Before each experiment, the transmittance

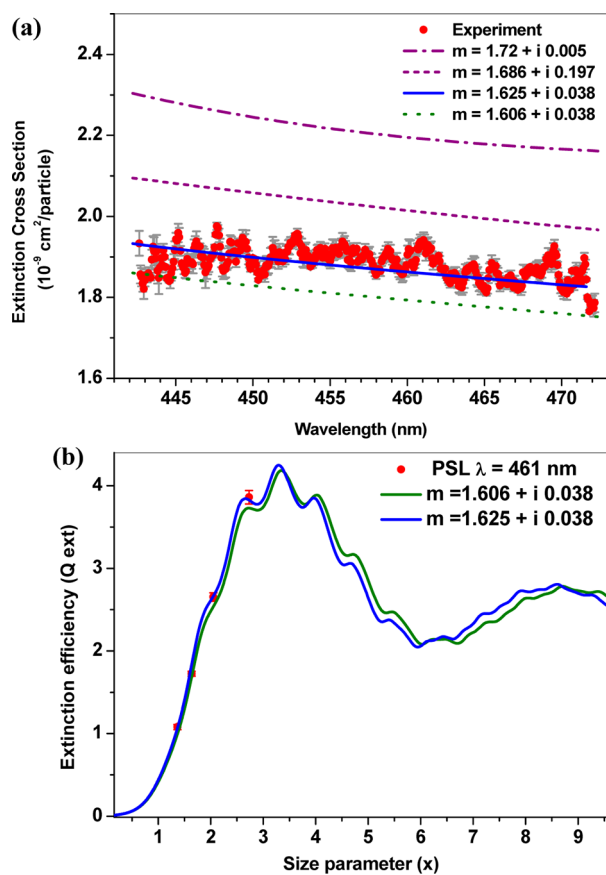


Figure 3. Refractive index retrieval: (a) extinction cross section (σ_{ext}) of 300 nm diameter polystyrene spheres (PSL) as a function of wavelength (λ). The experimental data and the measurement 1σ error are shown in red and gray, respectively. The blue solid curve represents the Mie fit: $m = 1.625 + i0.038$. The purple dash-dot line ($m = 1.686 + i0.197$), shot-dot line ($m = 1.72 + i0.005$), and olive dot line ($m = 1.606 + i0.038$) are from ref 42 at a wavelength of 335 nm, ref 41 at a wavelength of 335 nm, and ref 12 at a wavelength of 532 nm, respectively. (b) The extinction efficiency (Q_{ext} , the red dots) as a function of size parameter (x) of the PSL particle at 461 nm. The solid blue and green curves represent the Mie calculation with $m = 1.625 + i0.038$ and $m = 1.606 + i0.038$, respectively.

of a HEPA-filtered sample (particle free) was recorded as $I_0(\lambda)$. The retrieval algorithm of the refractive index was realized by fitting the measured wavelength-dependent extinction cross section ($\sigma_{\text{ext}} = \alpha_{\text{ext}}/N$) to the theoretically calculated cross section based on the Mie scattering subroutine, reported by Bohren and Huffman for homogeneous spheres.^{38,39} Best fit results were obtained by varying the real part of the RI. The imaginary part of the RI was fixed at the values recently reported by Abo Riziq et al.¹² and Bluvshstein et al.,¹⁸ from CRDS-based aerosol extinction measurements. A set of RI is found by minimizing the “merit function” χ^2/N^2 , where χ^2 is⁴⁰

$$\chi^2(n, D) = \sum_{j=1}^N \frac{[\sigma_{\text{ext,measd}}(n, \lambda_j, D) - \sigma_{\text{ext,theor}}(n, \lambda_j, D)]^2}{\epsilon_j^2} \quad (3)$$

The sum runs over all N spectral points, where n denotes the real parts of RI, and ϵ_j is the standard deviation of the measured extinction cross section.

Figure 3a shows retrieved refractive index based on the measured extinction cross section for a PSL particle. The purple dash-dot and shot-dot lines are the Mie theory calculated results with the RI values of $m = 1.72 + i0.005$ and $m = 1.686 + i0.197$ at 335 nm reported by Chartier and Greenslade⁴¹ and French et al.,⁴² respectively. The olive dot line is the calculated result with the RI value of $m = 1.606 + i0.038$ reported by Abo Riziq et al.¹² at 532 nm. The best fit result obtained from our experimental data was $m = 1.625 + i0.038$. This value obtained in the spectral region of 445–480 nm is well ranged between the reported RI values of $m = 1.686 + i0.197$ at 335 nm and $m = 1.606 + i0.038$ at 532 nm.

To evaluate the measurement accuracy of the retrieved RI from the IBBCEAS system, the traditional method comparing the measured extinction efficiency ($Q_{\text{ext}} = 4\sigma_{\text{ext}}/\pi D^2$) as a function of the size parameter (x) with the extinction efficiency calculated using the Mie scattering theory was used, as shown in Figure 3b. The experimental extinction efficiency (red dot) at 461 nm is presented for PSL with diameters of 200, 240, 300, and 400 nm, respectively. Two Mie theory results calculated with RI values of $m = 1.606 + i0.038$ (olive line) and $m = 1.625 + i0.038$ (blue line) are also shown in the figure. Good agreement between these data can be observed.

Sources of error and uncertainty in the RI retrieval have been discussed in detail by Miles et al.⁴³ for the case of using cavity ring-down spectroscopy to measure aerosol optical properties. The basic error sources include uncertainty in the determination of extinction cross section, uncertainties in particle size (including multiply charged particles) and in the cavity length d , as well as the efficiency of the CPC counting.

Supporting Information Figure S3 shows plots of the wavelength-resolved aerosol extinction cross section of 300 nm diameter particles calculated using Mie theory for various values of the RI real part (with fixed RI imaginary part). It shows that errors in the extinction cross section of $\pm 7\%$ can result in an error of $\pm 2\%$ in the retrieved real part of the RI.

Uncertainty in particle diameter is an important error source. A ± 5 nm uncertainty in particle diameter can lead to an error of up to $\pm 5\%$ in extinction cross section determination at $\lambda = 460$ nm (Supporting Information Figure S4), which can lead to an error in retrieved RI of $\sim \pm 1.5\%$. Size selection of aerosol particles used in the experiments was realized with a differential mobility analyzer (DMA) by which only aerosol particles of a given electrical mobility (or apparent mobility) diameter may be selected. The selection performance of the DMA was tested with certified PSL spheres with known size. The selected size of the particles can be determined by the peak position in the DMA signal which can be achieved by fitting a log-normal distribution to the measured DMA signal. The differences between the observed particle size and the certified diameters for the PSL spheres were within 1.7% (as shown in Supporting Information Figure S5).

DMA separates particles on the basis of their electrical mobility. The singly and doubly charged particles will have the same electrical mobility if the ratio of the respective mobility

diameters is ~ 1.5 . For example, both singly (100 nm) and doubly (150 nm) charged particles have the same electrical mobility diameters.⁴⁴ In general, there are singly and multiply charged particles emerging from the DMA selector, and multiply charged particles with large extinction cross section impact on the accurate measurement of aerosol property, which is needed to be well considered. Multiply charged particles were characterized by a tandem DMA (TDMA) method.⁴⁴ The size was selected with DMA-1 for 240 and 300 nm apparent mobility diameters. A second scanning DMA (DMA-2) was used for analysis of the component distributions of singly and multiply charged particles. Doubly charged particles from DMA-1 were not observed for PSL particles (Supporting Information Figure S6).

Supporting Information Figure S7 shows characterization of multiply charged particles of AS. Size distributions of AS with DMA-1 for 300 and 400 nm diameters are shown in Supporting Information Figure S7, parts a and b, respectively. For 300 nm apparent mobility diameter, the presence of doubly charged ($d_m \sim 450$ nm) in addition to singly charged particles emerging from DMA-1 was observed. The fraction of the doubly charged particles was about 7%. The extinction cross section of 450 nm diameter particles is about 4 times larger than that of the 300 nm diameter particles (assuming $m = 1.538 + i0.018$). Supporting Information Figure S7b shows that multiply charged particles were not presented for 400 nm AS apparent mobility diameter particles. The larger multiply charged particles were properly removed by inertial impaction at the inlet of the classifier. Size selection from polydispersed aerosol is very important to the retrieval of RI. The error of aerosol extinction cross section caused by the contribution of multiply charged particles was estimated to be between 5% and 20% for the particle diameters smaller than 300 nm, and less than 5% for the particle diameters larger than 400 nm.

Another key error source related to the present measurement system is the CPC counting efficiency. The over- or undercounting of the particle number density by the CPC would result in a systematic error in the value of the aerosol extinction cross section calculated from the experimental data. The counting efficiency of the used CPC (TSI 3775) was compared with another ultrafine CPC (TSI 3776). Both of them were well calibrated by the manufacturer. The number density measured by CPC 3776 was about 2.7% higher than that from CPC 3775.

The measurement precision of aerosol extinction cross section is shown in Figure 4. The data show 90 min of measurement of PSL particles with 300 nm diameter. The measured cross section was $1.83 \times 10^{-9} \text{ cm}^2/\text{particle}$ (with 1σ standard deviation of $9.4 \times 10^{-11} \text{ cm}^2/\text{particle}$; the corresponding relative uncertainty was about 5%), which agrees well with the Mie theory calculated value of $1.859 \times 10^{-9} \text{ cm}^2/\text{particle}$ with $m = 1.625 + i0.038$. A time series of N_2 extinction, as shown in the figure, was recorded to check the background drift during the extinction measurements. The 1σ standard deviation of $1.57 \times 10^{-9} \text{ cm}^{-1}$ in the background indicates high stability of the IBBCEAS system, which is comparable to the detection limit of the system for NO_2 detection.

The total uncertainty associated with the extinction cross section measurement was determined by the uncertainties in particle number concentration N and extinction coefficient α_{ext} . The propagating relative uncertainty is given by

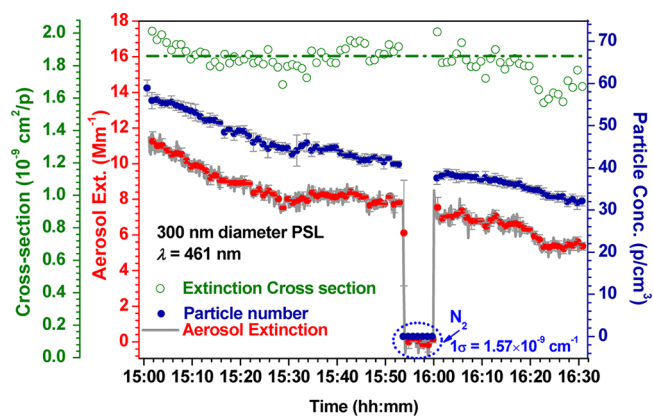


Figure 4. Single shot (9 s, gray line) and 1 min average (red full-filled circles) aerosol extinction (α_{ext}) measured for 300 nm PSL particles at 461 nm. Time series of N_2 extinction was also recorded to check the background drift. The 1σ standard deviation of $1.57 \times 10^{-9} \text{ cm}^{-1}$ represents good optical stability of the IBBCEAS spectrometer and the LED emission intensity. The particle number concentration (N , blue full-filled circles) was simultaneously measured. The aerosol extinction cross section (olive open circles) was calculated by α_{ext}/N . The measured extinction cross section of $1.83 \times 10^{-9} \text{ cm}^2/\text{particle}$ agrees well with the Mie theory calculation (dash dot line) value of $1.859 \times 10^{-9} \text{ cm}^2/\text{particle}$ with $m = 1.625 + i0.038$.

$$\frac{\Delta\sigma_{\text{ext}}}{\sigma_{\text{ext}}} = \sqrt{\left(\frac{\Delta N}{N}\right)^2 + \left(\frac{\Delta\alpha_{\text{ext}}}{\alpha_{\text{ext}}}\right)^2} \quad (4)$$

Each particle number concentration was acquired in 1 min with a mean measurement uncertainty of 3%. (The maximum and minimum measurement uncertainties were 8.3% and 1.2%, respectively.) The aerosol extinction coefficient was measured with an acquire time of 9 s (gray line in Figure 4); each 5–6 subsets were averaged (red dot, corresponding to an acquire time of ~ 1 min). A mean standard deviation of the extinction measurement was 3.7% (with a maximum value of 7.4% and minimum value of 1.4%, mainly caused by the particles' statistical noise and the occupancy of the particles in the light path). The calculated propagating uncertainty in the determined extinction cross section was 4.8%, which agrees well with the measurement uncertainty of 5%. After considering all the error sources mentioned above, for PSL particles, the total error in the used extinction cross section determination was about $\pm 7\%$, which can result in an error of about $\pm 2\%$ in the retrieved real part of refractive index.

Extending this analysis to field application, Figure 5 shows the measurement of AS aerosol mixed with filtered ambient air (containing NO_2). The relative humidity of the AS sample was controlled at $\sim 20\%$. As shown in Figure 5a, the contribution of 4.2 ppbv NO_2 to the extinction was about 8 Mm^{-1} . The H_2O absorption contribution was very small. The RI deduced from the fit of the measured extinction cross section was $m = 1.538 + i0.018$, which was close to the reported value of $m = 1.553 + i0$ and $m = 1.517 + i0.018$ at 355 and 532 nm (Figure 5b).¹⁸ This experiment shows that aerosol extinction coefficient and trace gases concentration could be simultaneously retrieved with high accuracy by the IBBCEAS approach.

Ambient Measurement. IBBCEAS measurement of ambient aerosol extinction and NO_2 was carried out for demonstration purposes during two representative days (June 6, cloudy day, and June 14, clear day). The measurements were

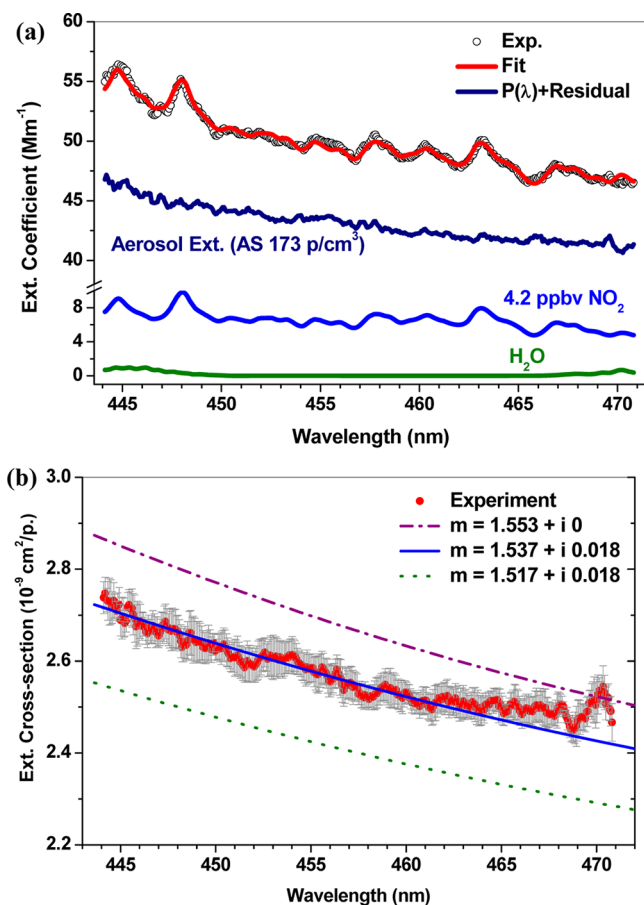


Figure 5. (a) Typical spectrum of the mixture of ammonium sulfate (AS) and particle-free filtered air. The experimental data and the fit are reported in the open black circles and red line, respectively; the reference spectra of NO_2 (corresponding to 4.2 ppbv) and H_2O are shown in the blue and olive lines, respectively. The aerosol extinction coefficient of AS (summation of $P(\lambda)$ and residual) is shown in the navy line. (b) The extinction cross section (σ_{ext}) of 350 nm AS particles as a function of wavelength (λ). The experimental data and the measurement 1σ error are shown in red and gray, respectively. The blue solid curve represents a Mie fit: $m = 1.538 + i0.018$. The purple dash dot line ($m = 1.553 + i0$) and olive dot line ($m = 1.517 + i0.018$) are from ref 18 at wavelengths of 335 and 532 nm, respectively.

taken outside the main building at Anhui Institute of Optics and Fine Mechanics ($31^\circ 54' 18'' \text{N}$, $117^\circ 9' 42'' \text{E}$). Sample was made by drawing ambient air in through Teflon tubing (10 mm inner diameter), about 7 m higher than ground level. A typical IBBCEAS spectrum of ambient air and the data retrieval is shown in Supporting Information Figure S8. The measured spectrum and the contributions of NO_2 , H_2O , and aerosol extinction are shown in the figure. RH of the ambient air was about 40% during the experiment. The IBBCEAS measured NO_2 data were compared to the values measured with an online NO_x analyzer (Thermo 42i). The correlation between these two data sets is plotted in the inset panel of Figure 6a. An enlarged drawing of the NO_2 measurement by IBBCEAS and the NO_x analyzer on June 14 is shown in Supporting Information Figure S9. The figure shows good agreement between the NO_x analyzer and the IBBCEAS measurements. Each data point was acquired in 9 s. Because of the lower time response of the NO_x analyzer (1 min), the NO_2 peaks were smoothed. The rapid fluctuation in NO_2 concentration could not be measured with the NO_x analyzer. A rapid NO_2

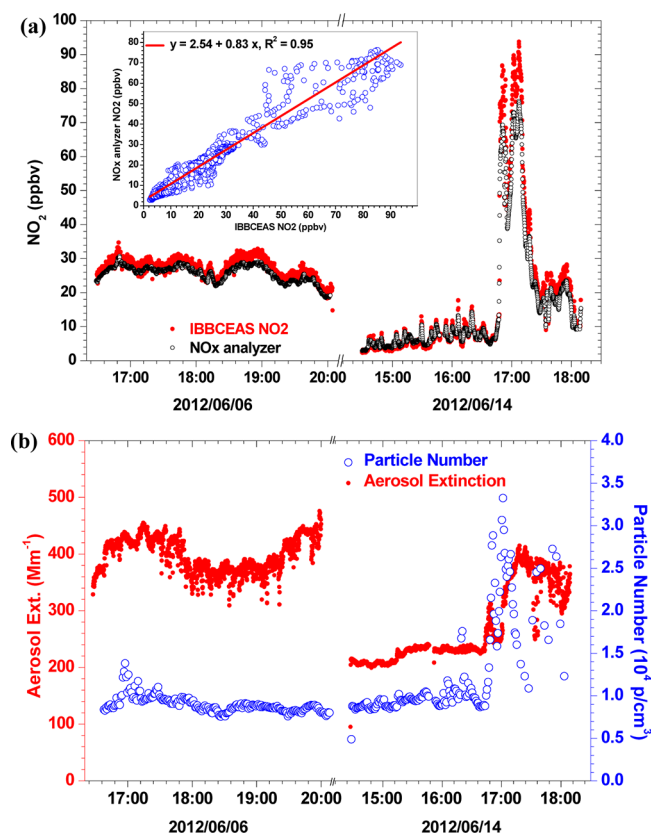


Figure 6. Ambient air measurements with the developed IBBCEAS spectrometer during two representative days (June 6, a cloudy day, and June 14, a clear day). (a) Intercomparison of NO_2 measurements with the IBBCEAS (red full-filled circles) and a chemiluminescence detector (black open circles). The measurements by the two instruments were each averaged over 9 s. A rapid change of NO_2 concentration was observed around 17:00 (local time) on June 14, 2012, which was mainly caused by traffic during the rush hour. The correlation between the two instruments is plotted in the inset panel showing good agreement ($R^2 = 0.95$). (b) Aerosol extinction coefficient of ambient air (red filled circles) at 461 nm and particle concentration measurement with a CPC. On June 14, the particle concentration and aerosol extinction were increased accompanied by a rapid increase of NO_2 concentration. The extinction coefficients of the two days were not proportional to aerosol number concentration, which may be caused by the different meteorological conditions and the different aerosol types of cloudy and clear days.

concentration change was observed around 17:00 (local time) on June 14, 2012, which was mainly caused by traffic during the rush hour. As shown in Figure 6b, during the rush hour, the particle number concentration was increased from 1×10^4 to 3×10^4 particles/ cm^3 . The aerosol extinction coefficient at 461 nm increased from 200 to 400 Mm^{-1} concomitant. The NO_2 concentration variation of ~ 80 ppbv might contribute about 144 Mm^{-1} to the extinction coefficient measurement if the gas absorption was not deconvoluted from the total measured extinction. This application to ambient air measurement demonstrated that the IBBCEAS technique provides a robust and convenient method for distinguishing aerosol extinction from gas absorption. The nonproportional aerosol extinction coefficients to the aerosol number concentration in the two days may be caused by the different meteorological conditions and the different aerosol types in cloudy and clear days. During the ambient measurement, the mirror reflectivity R was

calibrated once a day, and no deterioration of the mirror reflectivity was observed during 1 week of experiment.

CONCLUSIONS

In this paper, an LED-based IBBCEAS was built for measurement of wavelength-dependent aerosol extinction. The instrument was operated at the spectral range of 445–480 nm, with a detection limit of $1.45 \times 10^{-9} \text{ cm}^{-1}$ (1σ , 9 s). The measurement precision in aerosol extinction coefficient was 3.7%. The ambient air measurement shows that the contributions from gases absorption can be well identified among aerosol-induced optical extinction during the rush hour with fast change in NO_2 concentration.

In comparison to the single-wavelength instrument, broadband measurements provide a new approach for simultaneous quantification of both aerosol extinction and trace gases absorption, and meanwhile, this method provides a faster and more robust tool for retrieval of the real part of the aerosol RI. For determination of wavelength-dispersed RI by the IBBCEAS method, using multiple aerosol diameters at different wavelength would be adapted.

Retrieval of the imagined part of the aerosol RI needs additional scattering information. We focus in this work on the retrieval of the real part of the RI, and only nonabsorbing aerosols were measured and characterized. For further work, the optical scattering coefficient should be simultaneously measured to provide an efficient approach for faster retrieval of both real and imagined parts of the RI of different kinds aerosols: nonabsorbing as well as absorbing aerosols.^{11,45,46}

ASSOCIATED CONTENT

Supporting Information

Additional information as noted in text. This material is available free of charge via the Internet at <http://pubs.acs.org>.

AUTHOR INFORMATION

Corresponding Author

*E-mail: huangwei@aiofm.ac.cn (W.H.); wjzhang@aiofm.ac.cn (W.Z.).

Notes

The authors declare no competing financial interest.

ACKNOWLEDGMENTS

This research is supported by the National Natural Science Foundation of China (No. 41005017) and the Instrument Developing Project of the Chinese Academy of Sciences (YZ201121). The support of the Groupement de Recherche International SAMIA between CNRS (National Center for Scientific Research, France), RFBR (Russian Foundation for Basic Research, Russia), and CAS (Chinese Academy of Sciences, China) is acknowledged.

REFERENCES

- (1) Langridge, J. M.; Richardson, M. S.; Lack, D.; Law, D.; Murphy, D. M. *Aerosol Sci. Technol.* **2011**, *45* (11), 1305–1318.
- (2) Miles, R. E. H.; Rudić, S.; Orr-Ewing, A. J.; Reid, J. P. *Phys. Chem. Chem. Phys.* **2010**, *12* (5), 3914–3920.
- (3) Lack, D. A.; Richardson, M. S.; Law, D.; Langridge, J. M.; Cappa, C. D.; McLaughlin, R. J.; Murphy, D. M. *Aerosol Sci. Technol.* **2012**, *46* (5), 555–568.
- (4) Moosmüller, H.; Chakrabarty, R. K.; Arnott, W. P. *J. Quant. Spectrosc. Radiat. Transfer* **2009**, *110* (11), 844–878.

- (5) Sappey, A. D.; Hill, E. S.; Settersten, T.; Linne, M. A. *Opt. Lett.* **1998**, *23* (12), 954–956.
- (6) Smith, J. D.; Atkinson, D. B. *Analyst* **2001**, *126* (8), 1216–1220.
- (7) Strawa, A. W.; Castaneda, R.; Owano, T.; Baer, D. S.; Paldus, B. A. *J. Atmos. Oceanic Technol.* **2003**, *20* (4), 454–465.
- (8) Kebebian, P. L.; Robinson, W. A.; Freedman, A. *Rev. Sci. Instrum.* **2007**, *78*, 063102.
- (9) Massoli, P.; Kebebian, P. L.; Onasch, T. B.; Hills, F. B.; Freedman, A. *Aerosol Sci. Technol.* **2010**, *44* (6), 428–435.
- (10) Thompson, J. E.; Smith, B. W.; Winefordner, J. D. *Anal. Chem.* **2002**, *74* (9), 1962–1967.
- (11) Dial, K. D.; Hiemstra, S.; Thompson, J. E. *Anal. Chem.* **2010**, *82* (19), 7885–7896.
- (12) Abo Riziq, A.; Erlick, C.; Dinar, E.; Rudich, Y. *Atmos. Chem. Phys.* **2007**, *7* (6), 1523–1536.
- (13) Lang-Yona, N.; Rudich, Y.; Segre, E.; Dinar, E.; Abo-Riziq, A. *Anal. Chem.* **2009**, *81* (5), 1762–1769.
- (14) Moosmüller, H.; Varma, R.; Arnott, W. P. *Aerosol Sci. Technol.* **2005**, *39* (1), 30–39.
- (15) Strawa, A. W.; Elleman, R.; Hallar, A. G.; Covert, D.; Ricci, K.; Provencal, R.; Owano, T. W.; Jonsson, H. H.; Schmid, B.; Luu, A. P.; Bokarius, K.; Andrews, E. J. *Geophys. Res.* **2006**, *111*, D05S03.
- (16) Massoli, P.; Murphy, D. M.; Lack, D. A.; Baynard, T.; Brock, C. A.; Lovejoy, E. R. *Aerosol Sci. Technol.* **2009**, *43* (11), 1064–1074.
- (17) Spindler, C.; Abo Riziq, A.; Rudich, Y. *Aerosol Sci. Technol.* **2007**, *41* (11), 1011–1017.
- (18) Bluvshstein, N.; Flores, J. M.; Abo Riziq, A.; Rudich, Y. *Aerosol Sci. Technol.* **2012**, *46* (10), 1140–1150.
- (19) Fiedler, S. E.; Hese, A.; Ruth, A. A. *Chem. Phys. Lett.* **2003**, *371* (3–4), 284–294.
- (20) Thompson, J. E.; Spangler, H. D. *Appl. Opt.* **2006**, *45* (11), 2465–2473.
- (21) Varma, R. M.; Venables, D. S.; Ruth, A. A.; Heitmann, U.; Schlosser, E.; Dixneuf, S. *Appl. Opt.* **2009**, *48* (4), B159–B171.
- (22) Thalman, R.; Volkamer, R. *Atmos. Meas. Tech.* **2010**, *3* (6), 1797–1814.
- (23) Nakayama, T.; Sato, K.; Matsumi, Y.; Imamura, T.; Yamazaki, A.; Uchiyama, A. *Atmos. Chem. Phys. Discuss.* **2012**, *12*, 14551–14589.
- (24) Kraus, S.; Geyer, A. DOASIS Jscript programming description. <http://www.iup.uni-heidelberg.de/bugtracker/projects/doasis> (2001).
- (25) Fayt, C.; De Smedt, I.; Letocart, V.; Merlaud, A.; Pinardi, G.; Van Roozendael, M. QDOAS Software user manual. <http://uv-vis.aeronomie.be/software/QDOAS/index.php> (2011).
- (26) Bitter, M.; Ball, S. M.; Povey, I. M.; Jones, R. L. *Atmos. Chem. Phys.* **2005**, *5* (9), 2547–2560.
- (27) Ball, S. M.; Langridge, J. M.; Jones, R. L. *Chem. Phys. Lett.* **2004**, *398* (1–3), 68–74.
- (28) Gherman, T.; Venables, D. S.; Vaughan, S.; Orphal, J.; Ruth, A. A. *Environ. Sci. Technol.* **2008**, *42* (3), 890–895.
- (29) Ventrillard-Courtillot, I.; O'Brien, E. S.; Kassi, S.; Mejean, G.; Romanini, D. *Appl. Phys. B: Lasers Opt.* **2010**, *101* (3), 661–669.
- (30) Wu, T.; Chen, W.; Fertein, E.; Cazier, F.; Dewaele, D.; Gao, X. *Appl. Phys. B: Lasers Opt.* **2012**, *106* (2), 501–509.
- (31) Washenfelder, R. A.; Langford, A. O.; Fuchs, H.; Brown, S. S. *Atmos. Chem. Phys.* **2008**, *8* (24), 7779–7793.
- (32) Chen, J.; Venables, D. S. *Atmos. Meas. Tech.* **2011**, *4* (3), 425–436.
- (33) Naus, H.; Ubachs, W. *Opt. Lett.* **2000**, *25* (5), 347–349.
- (34) Sneep, M.; Ubachs, W. *J. Quant. Spectrosc. Radiat. Transfer* **2005**, *92* (3), 293–310.
- (35) Wu, T.; Zhao, W.; Chen, W.; Zhang, W.; Gao, X. *Appl. Phys. B: Lasers Opt.* **2009**, *94* (1), 85–94.
- (36) Vandaele, A. C.; Hermans, C.; Fally, S.; Carleer, M.; Colin, R.; Mérienne, M. F.; Jenouvrier, A.; Coquart, B. *J. Geophys. Res.* **2002**, *107*, 4348.
- (37) Kennedy, O. J.; Ouyang, B.; Langridge, J. M.; Daniels, M. J. S.; Bauguittie, S.; Freshwater, R.; McLeod, M. W.; Ironmonger, C.; Sendall, J.; Norris, O.; Nightingale, R.; Ball, S. M.; Jones, R. L. *Atmos. Meas. Tech.* **2011**, *4* (9), 1759–1776.

- (38) Bohren, C. F.; Huffman, D. R. *Absorption and Scattering of Light by Small Particles*; Wiley: New York, 1983.
- (39) Laven, P. MiePlot. <http://www.philiplaven.com/MiePlot.htm> (2006).
- (40) Dinar, E.; Riziq, A. A.; Spindler, C.; Erlick, C.; Kiss, G.; Rudich, Y. *Faraday Discuss.* **2008**, *137*, 279–295.
- (41) Chartier, R. T.; Greenslade, M. E. *Atmos. Meas. Tech.* **2012**, *5* (4), 709–721.
- (42) French, R. H.; Winey, K. I.; Yang, M. K.; Qiu, W. M. *Aust. J. Chem.* **2007**, *60* (4), 251–263.
- (43) Miles, R. E. H.; Rudić, S.; Orr-Ewing, A. J.; Reid, J. P. *Aerosol Sci. Technol.* **2011**, *45* (11), 1360–1375.
- (44) Bueno, P. A.; Havey, D. K.; Mulholland, G. W.; Hodges, J. T.; Gillis, K. A.; Dickerson, R. R.; Zachariah, M. R. *Aerosol Sci. Technol.* **2011**, *45* (10), 1217–1230.
- (45) Thompson, J. E.; Barta, N.; Policarpio, D.; DuVall, R. *Opt. Express* **2008**, *16* (3), 2191–2205.
- (46) Ma, L.; Thompson, J. E. *Anal. Chem.* **2012**, *84* (3), 5611–5617.